On the Nature of Small Planets around the Coolest *Kepler* Stars [1]

Eric Gaidos[2]

Department of Geology and Geophysics, University of Hawai'i at Mānoa, Honolulu, HI 96822

gaidos@hawaii.edu

Debra A. Fischer

Department of Astronomy, Yale University, New Haven, CT 06520

Andrew W. Mann

Institute for Astronomy, University of Hawai'i at Mānoa, Honolulu, HI 96822

and

Sébastien Lépine

Department of Astrophysics, American Museum of Natural History, New York, NY 10024

Received _____; accepted _____

Submitted to the Astrophysical Journal

[1]Some data were obtained at the W. M. Keck Observatory, which is operated by the California Institute of Technology, the University of California and NASA, and made possible by the financial support of the W. M. Keck Foundation.

[2]Visiting Professor, Pufendorf Institute, Lund University, Sweden

ABSTRACT

We constrain the densities of Earth- to Neptune-size planets around very cool (T_e=3660-4660 K) *Kepler* stars by comparing 1202 Keck/HIRES radial velocity measurements of 150 nearby stars to a model based on *Kepler* candidate planet radii and a power-law mass-radius relation. Our analysis is based on the presumption that the planet populations around the two sets of stars are the same. The model can reproduce the observed distribution of radial velocity variation over a range of parameter values, but, for the expected level of Doppler systematic error, the highest Kolmogorov-Smirnov probabilities occur for a power-law index $\alpha \approx 4$, indicating that rocky-metal planets dominate the planet population in this size range. A single population of gas-rich, low-density planets with $\alpha = 2$ is ruled out unless our Doppler errors are $\geq$5 m s^{-1}, i.e., much larger than expected based on observations and stellar chromospheric emission. If small planets are a mix of γ rocky planets ($\alpha = 3.85$) and 1-γ gas-rich planets ($\alpha = 2$), then $\gamma > 0.5$ unless Doppler errors are $\geq$4 m s^{-1}. Our comparison also suggests that *Kepler*'s detection efficiency relative to ideal calculations is less than unity. One possible source of incompleteness is target stars that are misclassified subgiants or giants, for which the transits of small planets would be impossible to detect. Our results are robust to systematic effects, and plausible errors in the estimated radii of *Kepler* stars have only moderate impact.

Subject headings: planetary systems — astrobiology — techniques: radial velocities

1. Introduction

The discovery of planets around other stars has placed our Solar System in context and stimulated speculation on the frequency of habitable planets and life in the Universe. Very cool dwarf stars (with late K and early M spectral types) are of special significance to such investigations because the two principle detection techniques, Doppler radial velocity (RV) and transit photometry, are more sensitive to smaller planets around smaller stars. Such stars are also much less luminous than solar-type stars, the circumstellar habitable zone is closer (Kasting et al. 1993), and planets within the habitable zone are therefore more detectable (Gaidos et al. 2007). These stars test models of planet formation: for example, core-accretion models predict fewer gas giants and more "failed" cores (Laughlin et al. 2004; Kennedy & Kenyon 2008), consistent with the lower frequency of giant planets and higher frequency of low-mass planets compared to G stars (Johnson et al. 2007; Cumming et al. 2008; Mayor et al. 2009). Finally, late K and early M dwarfs constitute three-quarters of all stars in the Galaxy, and their contribution weighs heavily in any cosmic accounting of planets or life.

Most confirmed exoplanets have been found by the Doppler technique, which can detect planets of a few Earth masses on short-period orbits around bright late F- to early K-type stars (Mayor et al. 2009; Howard et al. 2010). There are also Doppler searches for planets around very cool dwarfs (Zechmeister et al. 2009; Apps et al. 2010; Bean et al. 2010; Forveille et al. 2011). The CoRoT and *Kepler* missions have successfully extended the search for small planets to space using the transit technique. The *Kepler* spacecraft is monitoring ∼150,000 stars, including approximately 24,000 K-type stars and 3000 M-type stars (Batalha et al. 2010), and has discovered hundreds of candidate planets with radii R_p as small as ∼0.8 $R_\oplus$ (Borucki et al. 2011). The distribution with R_p peaks near $2R_\oplus$ and at the completeness limit of *Kepler* (Howard et al. 2011).

In principle, the mass M_p of a transiting planet can be uniquely determined by Doppler observations and mass and radii compared with theoretical relationships. The mean density of scores of giant planets and a handful of objects between the size of Earth and Neptune orbiting nearby stars have been determined in this manner (Gillon et al. 2007; Charbonneau et al. 2009; Hartman et al. 2011; Winn et al. 2011; Demory et al. 2011). This technique has also successfully confirmed candidate planets around the brightest CoRoT and *Kepler* stars, including two with masses only a few times that of Earth (Batalha et al. 2011; Hatzes et al. 2011). Comparison with a mass-radius relationship (MRR) can discriminate between denser planets composed of silicates and metal ("super-Earths"), and less dense planets with substantial envelopes of ices and hydrogen-helium gas ("ocean planets" or "mini-Neptunes") (Seager et al. 2007). However, the Doppler signal expected from many *Kepler* candidate planets is comparable to total instrument noise and stellar "jitter" (2-3 m s^{-1}, Figure 1). RV measurements can be "phased" to the transit-determined orbit, achieving greater sensitivity. Unfortunately, the great majority of cool *Kepler* stars are too faint ($K_p > 13$) to achieve the required high SNR even using 10-m telescopes.

Instead, Doppler observations of a sample of *nearby*, brighter stars can constrain the masses and mean densities of planets around corresponding *Kepler* stars, assuming both samples host the same planet population. Every planet will contribute to RV variance and the aggregate effect in excess of instrument errors and the noise from the stellar atmosphere ("jitter") can be detected. Given *Kepler*-determined orbits and planet radii and a hypothetical MRR, the cumulative distribution of RV variation can be predicted and compared to that from the nearby population. For a given distribution of observed radii, denser, rocky planets will generate greater RV variation, while less dense, ice- or gas-rich planets will produce smaller variation.

This approach exploits both the orbital information from *Kepler* and the collective RV

signal from the entire population. As with RV follow-up of individual transiting planets, planets are first detected by transit (*Kepler*), then characterized by Doppler observations. *Kepler* observations would provide an exact description of a equivalent nearby population only in the limit of an infinite sample, and thus the finite size of the candidate planet sample introduces uncertainty. We show that this uncertainty is not debilitating. This method also rests on two assumptions: (i) the planet populations of the Doppler and *Kepler* samples are statistically the same, and (ii) the MRR of small planets can be described by simple empirical relations. We discuss the validity of both of these assumptions.

We carry out such a combined transit-Doppler analysis, predicting the statistical distribution of RV variation in the M2K survey of late K and early M dwarfs (Apps et al. 2010). We use the *Kepler* distribution of candidate planet radii, corrected for detection efficiency, and assume a single parametric MRR. We compare the predicted and observed distributions to constrain the MRR and hence the compositions of the small planets these stars host.

2. Data

Doppler survey: The M2K survey has obtained 1406 RV measurements of 172 late K and early M dwarfs, with at least 3 measurements for each star. Stars were selected from the SUPERBLINK proper motion catalog (Lépine & Shara 2005) based on V-J color and parallax- or proper-motion-based absolute magnitudes (Lépine & Gaidos 2011), and confirmed by moderate-resolution spectroscopy. We excluded active stars with detectable emission in Hα or in the 90th percentile of emission in the HK lines of Ca II, and another 6 stars with problematic template spectra. The remaining stars are not exceptionally active, with median $R'_{HK} = -4.70$ and the vast majority have $-5 < R'_{HK} < -4.5$ (see inset in Figure 3). For stars with $B - V \approx 1$ these activity levels correspond to ages of 1-10 Gyr

(Mamajek & Hillenbrand 2008). Targets have apparent magnitudes of $V = 8 - 12$; most have $V = 9 - 10$.

Doppler spectra are obtained with the red channel of the HIRES spectrograph on the Keck I telescope (Vogt et al. 1994). Exposure times are adjusted to achieve SNR = 200. Absorption lines of molecular iodine are used as a rest-frame reference against which to measure the Doppler shift of features in the stellar spectrum. The shift is determined by minimizing the difference between the spectrum and a model combining an observed spectrum of the star without iodine and one of iodine imposed on the featureless spectrum of a B star (Marcy & Butler 1992; Butler et al. 1996). The error-weighted mean is subtracted from the measurements of each star and the RMS is calculated (Table 1).

The effective temperature T_e of each star is estimated from the V-K color and an empirical relation

$$\log T_e \approx 3.9653 - 0.164(\mathrm{V} - \mathrm{K}) + 0.0168(\mathrm{V} - \mathrm{K})^2, \quad (1)$$

which has an accuracy of 1% (Benedetto 1998). We estimate stellar mass M_* using an empirical relation $\log(M_*/M_\odot) = 1.5 \log(T_e/5780) + 0.02$ based on a Yale-Yonsei 5 Gyr isochrone (Demarque et al. 2004). The metallicites of 95 stars have been estimated using the Spectroscopy Made Easy code (Valenti & Piskunov 1996). The standard deviation of [Fe/H] in our sample is ± 0.21 dex, and the concomitant error in stellar mass due to the use of a solar-metallicity isochrone is $\sim 0.02 \mathrm{M}_\odot$, which we ignore.

Kepler targets and planets: We use the Quarter 2 *Kepler* target list from the Multimission Archive (STScI). *Kepler* candidate planets are taken from Borucki et al. (2011), who report R_p based on stellar radius R_*, the orbital period P, and the estimated T_e and surface gravity $\log g$ of the host star. Stellar parameters are based on the multi-passband photometry and Bayesian analysis of the Kepler Input Catalog (KIC) Brown et al. (2011). We consider only putative dwarf stars with $4 < \log g < 4.9$.

Effective temperature range: We choose a T_e range that includes a substantial number of stars from each sample and maximizes the similarity in the temperature distributions as assayed by the Kolmogorov-Smirnov (K-S) statistic. For an interval of 1000 K, that range is 3660-4660 K (K-S probability = 4.7×10^{-3}). This includes 150 M2K stars (1202 measurements) and 10,018 *Kepler* target stars, the latter having 138 candidate planets, and excludes the 410 very coolest *Kepler* target stars and 6 hotter M2K stars. The mean effective temperatures of the M2K and *Kepler* subsamples are 4230 K and 4200 K, respectively. The low K-S probablity reflects the narrower distribution of M2K stars within this range of T_e compared to the *Kepler* sample (Figure 2). We speculate on the possible impact of this difference on our analysis in Section 6.

3. Model

Planet frequency: The expected frequency of the ith planet candidate in the *Kepler* survey is $1/s_i$, where $s_i = \Sigma_j p_{ij} q_{ij}$, p_{ij} is the geometric probability of a transiting orbit around the jth star, and q_{ij} is the probability of detection if the planet is on a transiting orbit. s_i is the expected number of stars around which a planet would be detected, if every star had this planet on its particular orbit. For example, a planet that could have been detected around 100 stars, but has been found once, has a most likely occurence rate of 1%. For planets that are small compared to their host stars and on nearly circular orbits, the transit probability is:

$$p = 0.238 F P^{-2/3} M_*^{-1/3} R_*, \tag{2}$$

where P is in days and $F = T/P$ if $P > T$, where T is the observation period (120 d), or else $F = 1$. M_* and R_* are in solar units. A planet is detected if $SNR = \delta/\sigma \geq 7$ (Borucki et al. 2011), where δ is the transit depth and σ is the noise over the entire transit. In our Monte Carlo calculations (see below) q_{ij} only takes on values of 0 or 1 depending on

whether $SNR \lesseqgtr 7$. Assuming uncorrelated noise,

$$SNR = \frac{\delta}{\sigma_{30}} \sqrt{\frac{N\Delta}{30}}, \tag{3}$$

where σ_{30} is the noise per 30-minute integration, N is the number of observed transits, and Δ is the transit duration in minutes. The transit depth is $\delta \approx 8.4 \times 10^{-5} (R_p/R_*)^2$, where R_p is in Earth units. The noise per 30-min integration as a function of *Kepler* magnitude K_P is $\sigma_{30} \approx 10^{(K_P-13)/5-4}$ (Koch et al. 2010). We multiply this by a factor drawn randomly from the distribution in Figure 4 of Koch et al. (2010) to account for stellar variability. Stars with factors > 10 are assigned a factor of 10. The number of observed transits is the largest integer less than T/P. (Three cases where $P > T$ and $N = 1$ were confirmed by the *Kepler* team using later observations.) The transit duration for a circular orbit, averaged over all possible impact parameters, is

$$\tau \approx 85 R_* M_*^{-1/3} P^{1/3} \text{min}. \tag{4}$$

To account for incompleteness or overestimation of the detection efficiency of *Kepler*, we multiply s_i by a constant parameter C, where $0 < C \leq 1$. We use a single, uniform value for detection efficiency both as a necessary simplification and because it can describe one possible cause of detection inefficiency - the presence of giant stars in the target list (Section 4). We do not correct for false positives, probably 5-10% (Morton & Johnson 2011). $C > 1$ is possible but unlikely if the false-positive rate is low, and we do not consider values of $C < 0.2$.

Mass-radius relations: For the MRR of planets with $R_p > 3\text{R}_\oplus$, i.e. Neptune size or larger, we use the masses and radii of 120 confirmed transiting planets (Schneider et al. 2011). M_p is calculated using the mean density of the 8 such planets with radii closest to that of the *Kepler* object. Smaller planets with radii $\leq 3\text{R}_\oplus$ are described by a single population with $M_p = R_p^\alpha$ (Earth units). Although the MRRs of solid planets

(rock/ice/metal) are not expected to precisely follow power laws (Fortney et al. 2007; Seager et al. 2007), a power law with $\alpha \approx 3.85$ is a reasonable approximation for a planet with an Earth-like ratio of silicates to metal, and little gas. If planets have acquired and retained a substantial H-He envelope, and the mass fraction of the envelope increases with M_p, we expect $\alpha \ll 4$. For example, $M_p \sim R_p^2$ describes a continuum between Earth and Neptune, and gas-rich super-Earths may have $\alpha \leq 0$ (Rogers et al. 2011). Of course, the small planets may be a mix of both rocky- and gas-rich objects and we entertain this scenario in Section 4.

Radial velocity errors: Appropriate modeling of RV errors is crucial to this analysis. The median standard deviation of formal (including Poisson) errors is 1.3 m s^{-1}, and we use the actual formal errors in our calculations. Fifteen pairs of RV measurements taken within 6 hr show additional total systematic error of ≈ 3 m s^{-1}. We assume that additional systematic instrument errors and stellar noise ("jitter") are uncorrelated between observations and gaussian-distributed, but we examine the effect of correlated instrument errors in Section 5. For instrument noise we use a fixed RMS of 1.6 m s^{-1} based on observations showing this to be the "basement" level of systematic noise among a large number of HIRES observations of K stars (Isaacson & Fischer 2010). Stars do not exhibit a monotonic level of jitter. Figure 3 shows the distribution of total systematic noise (instrument plus stellar jitter) predicted for 100 M2K stars based on their Ca II HK emission, B-V colors, and the equations in Isaacson & Fischer (2010). We adopt a Rayleigh formula for the distribution of the jitter RMS σ_* among all stars in the sample,

$$p(\sigma_*) = \frac{\sigma_*}{\sigma_0} \exp\left(\frac{-\sigma_*}{\sigma_0}\right), \tag{5}$$

where we term σ_0 the *magnitude* of the jitter. (In Section 5 we also try an exponential distribution.) The RMS jitter in an *ensemble* of stars with a Rayleigh distribution is $\sqrt{2}\sigma_0$. Our 6 hr systematic noise level of 3 m s^{-1} can be explained if $\sigma_0 = 1.8$ m s^{-1}. The

predicted jitter distribution is best described by $\sigma_0 = 1.7 \pm 0.1$ m s^{-1} (Figure 3), consistent with our observations of 3 m s^{-1} total RMS . Additional noise due to stellar rotation and starspots may occur on longer timescales (Barnes et al. 2011), and we perform calculations with σ_0 over the range 1.5-4.5 m s^{-1}. However, we consider values near the upper limit, corresponding to an average systematic noise of 6.5 m s^{-1}, highly implausible because of the absence of active stars in in our sample (inset of Figure 3). This is discussed further in Section 6.

Radial velocity calculations: We predict the distribution of RV RMS for each set of parameter values by generating 10,000 Monte Carlo systems, with host stars selected with replacement from the M2K survey, and orbital inclinations drawn from an isotropic distribution. Each *Kepler* candidate planet has a probability $1/s_i$ of being added to each star. This ignores any autocorrelation between the presence of planets. Masses are assigned to each planet using the *Kepler* radius and the MRR. We ignore all planet candidates with radii larger than the largest confirmed transiting planet ($\sim$2 Jupiter radii) as main sequence companions or false positives. The RV variation induced by each planet is calculated from the planet mass, host star mass, and system inclination. Orbits are assumed to be approximately coplanar (Lissauer et al. 2011). Radial velocities are calculated using the actual epochs of observations and random mean anomalies at the first epoch. We draw longitudes of perihelion from a uniform distribution and orbital eccentricities from a Rayleigh distribution with mean of 0.225 (Moorhead et al. 2011). We add formal and systematic errors to the simulated radial velocities, subtract the error-weighted mean, and calculate the RMS. To filter binary stars, we remove observed and predicted systems whose RMS exceeds a specified cutoff B.

Statistical comparison: The model and observed distributions are compared using the two-sided Kolmogorov-Smirnov (K-S) test and the two-sample Kuiper test; the latter is

sensitive to the tails of a distribution as opposed to the median. The four parameters of the model are the MRR parameter α, jitter magnitude σ_0, binary cutoff B, and completeness C. In Section 4 we introduce a fifth parameter γ that describes a mixed population of rocky and Neptune-like planets.

4. Results

A byproduct of our analysis is an estimate of the average number of planets per star: $\sum_i s_i^{-1}$. We find that 30% of *Kepler* stars with T_e = 3660-4660 K have planets with $R_e > 2\mathrm{R}_\oplus$ and $P < 50$ d. This is in agreement with the findings of of Howard et al. (2011). The frequency of giant planets ($R_p > 0.8R_J$) in our sample is 2.4%, close to that estimated in Doppler surveys (Johnson et al. 2010). This indicates minimal bias in our Monte Carlo reconstruction of the discrete *Kepler* sample because any effect should be most pronounced for the rarest (largest) planets.

The observed cumulative distribution of RV RMS (points in Figure 4) has an accelerating rise below 3 m s^{-1} from gaussian noise, a logarithmic increase over 3-10 m s^{-1} from the combined effect of systematic error and planets not resolved by Doppler observations, and a tail beyond 10 m s^{-1} from giant planets and low-inclination binary stars. The best-fit models (e.g., solid line) agree with the observed distribution with a K-S probability >90%. The K-S and Kuiper statistics are largely congruent and hereafter we show only the former. 95% confidence intervals in the uncertainty due to the finite size of the *Kepler* planet sample were calculated using 200 bootstrap-resampled planet populations and are plotted as dashed lines in Figure 4. (These illustrate deviations from the best-fit cumulative distribution, and are not cumulative distributions themselves, which can never reverse). The high RMS tail of the distribution contains few systems and is most poorly reproduced.

Jitter magnitude, completeness, and MRR parameter α influence the predicted distribution of RV variation in similar ways, and different combinations of parameter values can reproduce the observations. Values that produce high K-S probabilities describe a locus in $C - \alpha - \sigma_0$ space. In contrast, our results are insensitive to the binary cutoff B for reasonable values; $B = 110$ m s^{-1} is used in all analyses. This value excludes 24 systems and implies that $\sim 70\%$ of M2K stars are single. This is an upper limit because M2K excludes known spectroscopic and close (< 2 arc-sec) binaries, and is not sensitive to wide (but unresolved) binaries. This fraction is intermediate the single star fraction of 40% for G stars and 80% for M stars (Lada 2006).

We first performed calculations assuming $C = 1$ and allowing α to vary from 2 to 5, and σ_0 to vary from 1.5 to 4.5 m s^{-1}. This range of σ_0 is intended to capture the locus of high K-S probabilities over the entire plausible range of α; high values of σ_0 clearly contravene our observations and predictions based on chromospheric emission (Figure 3). Contours of 0.01, 0.05, 0.1, and 0.5 probability, corresponding to confidence intervals of 99%, 95%, 90% and 50%, are plotted in Figure 5a. The location of maximum K-S probability is marked as an "x", but we caution against overinterpretation of this location because even the contour of lowest confidence (50%) is very broad.

If the detection efficiency is near unity for these stars, agreement between *Kepler* and Doppler observations favors a high α but also demands implausibly high values of σ_0. Better reconciliation between *Kepler* and Doppler can be achieved if *Kepler* detections are incomplete relative to the idealized calculations for these stars, i.e. if $C < 1$. If $C = 0.5$, then $\sigma_0 \sim 2$ m s^{-1} permits values of $\alpha \sim 4$, but not much lower values: values of $\alpha \leq 2$ are possible only if $\sigma_0 > 3.2$ m s^{-1}(total systematic noise > 4.8 m s^{-1}) at 99% confidence (Figure 5b).

One cause of $C < 1$ may be interloping giant stars in the target list (Basri et al. 2011).

Giant stars have radii $\geq 10R_{\odot}$, and the transits of planets even as large as Neptunes will be ≤ 12 ppm and undetectable by *Kepler*, especially with the confounding effect of oscillations (Huber et al. 2010). There is indirect evidence for such contamination in the distribution of planet candidates with stellar colors. Figure 6 plots the $g-r$ (SDSS) and $J-K$ (2MASS) colors of *Kepler* target stars from the KIC (Brown et al. 2011). Yellow and red points have estimated surface gravities $4 < \log g < 4.9$ (putative main sequence stars) and $\log g < 4$ (putative subgiants and giants), respectively. Black contours are lines of constant (sub)giant fraction. Purple points mark candidate planet hosts. The green contour encloses 90% of stars with T_e=3660-4660 K. Planet-hosting stars are conspicuously sparse in the vicinity of $J-K \approx 0.7$ and $g-r \approx 0.9$, where the fraction of (sub)giants exceeds 50%. Many putative K dwarf stars in this region of color space may instead be misclassified (sub)giants, with much larger radii and higher variability.

We also evaluated the range of (σ_0,α) parameter space over which the specific scenarios of rock-metal planets ($\alpha = 3.85$) and gas/ice-rich planets ($\alpha = 2$) are allowed (Figures 5c and d). The former is permitted by a plausible range of σ_0 for $C < 1$, with $C = 0.4$-0.5 being most consistent with our Doppler data. All cases with $\alpha = 2$ are ruled out at >95% confidence as long as $C > 0.2$ and $\sigma_0 \leq 2.4$ m s^{-1}(total systematic noise ≤ 3.8 m s^{-1}).

Small planets may instead comprise an admixture of rocky, ice-rich, and gas-rich worlds. Wolfgang & Laughlin (2011) find evidence for a mixed population around solar-type stars. We considered this scenario by assuming that the population consists of a mixture of $\alpha = 3.85$ and $\alpha = 2$ planets with frequency γ and $1-\gamma$, respectively. The K-S probability distribution vs. σ_0 and γ is plotted in Figure 7. The maximum K-S probability (93%) occurs for $\gamma = 0.88$ and $\sigma_0 = 2.8$ m s^{-1}, but a range of correlated γ and σ_0 values are possible. If σ_0 is not much larger than 2 m s^{-1} then values of γ near unity are clearly favored, and if $\sigma_0 < 2.6$ m s^{-1} (<4 m s^{-1} total systematic Doppler error) then $\gamma > 0.5$ at

99% confidence.

5. Sensitivity to Model Assumptions

We performed a series of calculations to test the sensitivity of our results to some assumptions of the model. We considered the $C = 0.5$ case, and thus outcomes should be compared to Figure 5b.

Distribution of jitter RMS: We replaced the Rayleigh distribution of jitter RMS σ_0 with an exponential distribution, while maintaining the same ensemble RMS. This modification shifts the locus of acceptable models to values slightly lower values of α and sightly higher values of σ_0 (Figure 8a), but otherwise does not significantly impact our results.

Correlated noise: Correlated or "red" instrument noise in Doppler observations does not decrease as the square root of the number of measurements, making *de novo* detections of signals comparable to such noise very difficult. This has little impact on our results because they rely on *Kepler* for planet detections and we analyze only the variance (total power) of the RV, a quantity independent of the noise spectrum. Correlated noise would only be important if there was significant drift of HIRES measurements on timescales longer than the timespan of our measurements (months to years). Long-term monitoring of RV-stable stars rules out such behavior, e.g. Apps et al. (2010). We further tested the possible effect of red noise on our analysis by modeling instrument noise as correlated with a power spectrum $exp(-\omega\tau)$, where τ is the noise coherence time. Uncorrelated ("white") noise values w_i at times t_i are replaced by "red" noise values r_i where

$$r_i = \sum_j \frac{w_j}{1 + \left[2\left(t_i - t_j\right)/\tau\right]^2}, \tag{6}$$

and the sum is over *all* observations, whether they are of a given star, or not. In calculating reddened instrumental noise, we use the actual epochs of the observations t_i. Errors are

then re-normalized to keep the variance the same. The coherence time of HIRES instrument noise is not known but we assume $\tau = 20$ d. Figure 8b shows that the impact on our results is very small.

Random errors in KIC radii: Inferences about densities and a mass-radius relationship depend sensitively on *Kepler*'s estimates of planet radii, which are uncertain. To investigate the effect of random errors, we added gaussian-distributed errors with 25% RMS to the *Kepler* radii. This modification broadens the locus of acceptable parameter values and shifts the best-fit models to slightly lower α and slightly higher jitter, but otherwise does not significantly impact our results (Figure 8c).

Systematic errors in KIC radii: The astroseismically-determined radii of many *Kepler* solar-type stars are systematically larger (a median of 20%) than KIC estimates (Verner et al. 2011). If this were also the case for the late K and early M stars in our sample, the planets they host would be larger by the same amount, and hence less dense. If the effect is uniform, the inferred frequency of planets, which depends mostly on detectability, transit depth and hence the ratio of radii, is largely unchanged. We investigated this scenario by increasing the radii of all stars and planets by 20% (Figure 8d). Larger planet radii and lower densities shift the locus of permissable α and σ_0 to only slightly lower values. On the other hand, Muirhead et al. (2011) point out that a stellar evolution model predicts consistently *smaller* radii for planet-hosting M dwarfs compared to KIC estimates. A running median of KIC radii vs. effective temperature, reduced by 15%, is roughly consistent with a Yale-Yonsei 5 Gyr solar-metallicity isochrone. We therefore performed a second analysis in which star and planet radii were uniformly decreased by 15% (Figure 8d). As expected, this shifts the locus to both higher α and σ_0. As we discuss below, systematic overestimation of stellar radius and the presence of interloping giant stars may not necessarily be incompatible.

6. Discussion

Our combined analysis of *Kepler* transit detections and Doppler radial velocities for late K and early M stars finds that consistency is possible for a wide but not unlimited range of parameters. As expected for an analysis based on RV variance, there is an inverse relationship between acceptable values of planet mass, i.e., the power-law index α of the planet mass-radius relation, and stellar jitter, i.e. the parameter σ_0 that characterizes its distribution among stars. However, if the level of radial velocity jitter in M2K stars is as expected, reconciliation of *Kepler* and Doppler observations can only be achieved if $\alpha \sim 4$, and $\alpha \sim 2$ is excluded. In other words, small planets around these stars are primarily rocky-metal "super-Earths" rather than hydrogen gas-rich "mini-Neptunes". We cannot absolutely rule out higher jitter ($\sigma_0 \geq 3$ m s^{-1}, corresponding to total systematic RMS > 4.5 m s^{-1}) that would admit a lower value of α, but there is no evidence to support such a choice. Instead, $\sigma_0 \sim 2$ m s^{-1} is supported by the RMS of our paired Doppler observations, the predicted stellar jitter based on chromospheric activity and the observed levels of jitter among other, similar stars (Apps et al. 2010; Isaacson & Fischer 2010). Our choice of $\alpha = 2$ to represent gas-rich planets is conservative because theoretical modeling suggests values closer to zero or even negative over the mass range of interest (Rogers et al. 2011).

Reconciliation of *Kepler* and Doppler data, even with $\alpha \sim 4$, also appears to require that *Kepler*'s detection efficiency be less than unity and perhaps ∼50%. Some of this incompleteness could arise if many target stars are misclassified subgiant or giant stars around which Neptune-size or smaller planets are difficult or impossible to detect by *Kepler*. Spectroscopic follow-up finds that essentially all late K and M *Kepler* stars brighter than $K_p = 14$ are giants (Mann et al., in prep.); we estimate the rate of interlopers in our sample of *Kepler* targets to be at least 15%. Giant interlopers are rare among the transiting planet-hosting *Kepler* stars (Muirhead et al. 2011) because the vast majority of planets

are smaller than Jupiter and not detectable around giant stars. Additional incompleteness could come from higher stellar variability.

Our analysis appears robust to the precise choice of function for the distribution of jitter RMS among stars, as long as the overall noise variance is conserved. It is also insensitive to the presence of correlated or "red" noise in the Doppler RV data. Although our results are not overly susceptible to random errors in estimated stellar radii, they do vary with uniform systematic errors in those values. If radii have been uniformly overestimated, as comparisons with stellar evolution models suggest, agreement between *Kepler* and M2K statistics favors a slightly higher value of α, reinforcing our conclusion that the small planets around these stars are primarily rocky. Although the resulting offset of the locus with α may seem small, one property of a power-law MRR is that a compensatory fractional change in index α will equal the fractional magnitude of a systematic change in radius, modulo a logarithmic factor which is approximately unity. For example, if radii are 15% smaller then α should be 4.6 instead of 4.

Systematic underestimation of stellar radii can be reconciled with the presence of interloping giant stars by accounting for strong selection effects among stars with transit-detected planets: Just as transit surveys of a given set of stars are biased towards the largest planets (Gaudi 2005), a given set of planets will be more readily detected by transit around the smallest stars in a sample; stars with detected planets are thus not necessarily representative of the entire sample. Reliable estimates of the radii of a presentative sample of late-type *Kepler* target stars should be vigorously pursued.

Our analysis is predicated on statistically indistinguishable planet populations in our samples of stars from the *Kepler* field and solar neighborhood. A plausible condition for this assumption is that the two samples have similar mass and metallicity distributions and be drawn from the same stellar population. The effective temperature distributions

are similar, but not identical (Figure 2) and this may translate into differences in stellar mass. There is an excess of about 30 M2K stars (∼20% of the sample) around 4200 K and a deficit around 3850 K. According to a Yale-Yonsei 5 Gyr solar-metallicity isochrone, this 350 K increase corresponds to changing the stellar mass from $0.57M_{\odot}$ to $0.65M_{\odot}$. Adopting the relation between stellar mass and giant planet frequency of Johnson et al. (2010) at face value, these M2K stars would have a 14% higher incidence of giant planets, but the giant planet frequency in the overall sample would only be 3% higher. According to Equation 9 in Howard et al. (2011) the frequency of *all* planets would decrease by 6%.

M2K stars are all within 45 pc of the Sun, and the median distance is 25 pc, placing them well within the galactic disk. These stars are drawn from a proper motion-selected catalog (>40 mas yr^{-1}) with a transverse velocity limit of 8.6 km s^{-1} at 45 pc (Lépine & Shara 2005). The velocity dispersion of stars in the solar neighborhood is anisotropic but a rough estimate of 80% completeness at 45 pc is obtained by assuming an isotropic distribution with a dispersion of 25 km s^{-1} (Bond et al. 2010). The correlation between metallicity and velocity dispersion (via age) means that this sample will be biased against metal-rich stars, but this effect is very small: Stars with [Fe/H]=-0.5 (more metal-poor stars are very uncommon) have a velocity dispersion ∼5 km s^{-1} higher than their solar metallicity counterparts (Lee et al. 2011), and the corresponding completeness is ∼84% at 45 pc. The bias against solar-metallicity stars in M2K is therefore ≤5%. Although we excluded the most active stars from the analysis and may have removed any very young stars, this should not affect the metallicity distribution because the metallicity-age relation is flat in this range (Holmberg et al. 2007). Tidal decay of the orbits of low mass planets around small stars is expected to be extremely slow (Jackson et al. 2009) and would not appreciably evolve a planet population.

The kinematics and metallicities of *Kepler* field stars have yet to be established. The

center of the *Kepler* field ($l = 77°$, $b = +13°$) is nearly perpendicular to the direction to the galactic center, and approximately parallel to the galactic plane. We estimate photometric distances from *Kepler* derived temperatures using the empirical relation for absolute magnitude $M_J \approx 6.25 - 16.53 \log(T_e/4000)$. At the median estimated distance of the subsample (256 pc), a star at the center of the *Kepler field* has approximately the same galactocentric distance as the solar neighborhood and is only ∼60 pc above the galactic plane; most stars should belong to the thin disk and have near-solar metallicities. Consistent with this, the TRILEGAL stellar population model (Vanhollebeke et al. 2009) predicts that only 7% of stars in this range of effective temperature and magnitude belong to the thick disk or halo, and only 6% have [Fe/H] < -0.5. Thus we conclude that the *Kepler* and M2K samples are very similar in mass, metallicity, and age.

Howard et al. (2011) estimated planet densities by comparing distributions of *Kepler* radii with masses from a Doppler survey of solar-type stars. They inferred a higher density for the smallest planets, consistent with our findings. Wolfgang & Laughlin (2011), using a different set of Doppler-detected planets, also concluded that the majority of small planets around solar-type stars are rocky. They also found that the proportion of low density, gas-rich planets increases with planet size, a feature essentially intrinsic to our analysis because of our choice of $\alpha = 2$. Theoretical models predict the formation of inner, rocky planets (Raymond et al. 2004), and the stellar UV-driven escape of any primordial hydrogen atmospheres (Pierrehumbert & Gaidos 2011). The low density of the short-period super-Earth GJ 1214b can be explained by a substantial hydrogen envelope (Charbonneau et al. 2009; Croll et al. 2011), but also by a thick H_2O shell (Bean et al. 2010a; Désert et al. 2011). Its host is a cooler (3000 K), much less luminous mid-M star and this may permit retention of hydrogen (Pierrehumbert & Gaidos 2011). Gas- and ice-rich planets resembling GJ 1214b may be the exception rather than the rule around the coolest *Kepler* target stars. Refinement of Doppler systematic errors and the properties of *Kepler*

target stars, specifically the radii of K and M dwarfs and the fraction of interloping giants, will permit more robust constraints.

This research was supported by NSF grants AST-09-08406 (EG), AST-10-36283 (DAF), AST-09-08419 (SL); NASA grants NNX10AI90G and NNX11AC33G (EG), and the NASA KPDA program (DAF). The *Kepler* mission is funded by the NASA Science Mission Directorate, and data were obtained from the Multimission Archive at the Space Telescope Science Institute, funded by NASA grant NNX09AF08G. We thank Andrew Howard for his help with screening Doppler template spectra.

REFERENCES

Apps, K., et al. 2010, PASP, 122, 156

Barnes, J. R., Jeffers, S. V., & Jones, H. R. A. 2011, MNRAS, 412, 1599

Basri, G., et al. 2011, AJ, 141, 20

Batalha, N. M., et al. 2010, ApJ, 713, L109

Batalha, N., et al. 2011, ApJ, 729, 27

Bean, J. L., Seifahrt, A., Hartman, H., Nilsson, H., Wiedemann, G., Reiners, A., Dreizler, S., & Henry, T. J. 2010, ApJ, 713, 410

Bean, J. L., Kempton, E. M.-R., & Homeier, D. 2010a, Nature, 468, 669

Benedetto, G. D. 1998, A&A, 871, 858

Bond, N. a., et al. 2010, ApJ, 716, 1

Borucki, W. J., et al. 2011, ApJ, 736, 19

Brown, T., Latham, D., Everett, M., & Esquerdo, G. 2011, AJ, 142, 112

Butler, R. P., Marcy, G. W., Williams, E., McCarthy, C., Dosanjh, P., & Vogt, S. S. 1996, PASP, 108, 500

Chabrier, G., & Baraffe, I. 2000, ARA&A, 38, 337

Charbonneau, D., et al. 2009, Nature, 462, 891

Croll, B., Albert, L., Jayawardhana, R., Miller-Ricci Kempton, E., Fortney, J. L., Murray, N., & Neilson, H. 2011, ApJ, 736, 78

Cumming, A., Butler, R. P., Marcy, G. W., Vogt, S. S., Wright, J. T., & Fischer, D. A. 2008, PASP, 120, 531

Demarque, P., Woo, J., & Kim, Y. 2004, ApJSS, 155, 667

Demory, B.-O., et al. 2011, A&A, 533, A114

Désert, J.-M., Kempton, E. M.-R., Berta, Z. K., Charbonneau, D., Irwin, J., Fortney, J., Burke, C. J., & Nutzman, P. 2011, ApJ, 731, L40

Fortney, J. J., Marley, M. S., & Barnes, J. W. 2007, ApJ, 659, 1661

Forveille, T., et al. 2011, A&A, 526, A141

Gaidos, E., Haghighipour, N., Agol, E., Latham, D., Raymond, S. N., & Rayner, J. 2007, Science, 318, 210

Gaudi, B. S. 2005, ApJ, 628, L73

Gillon, M., et al. 2007, A&A, 472, L13

Hartman, J., et al. 2011, AJ, 728, 138

Hatzes, A., et al. 2011, arXiv:1105.3372

Holmberg, J., Nordström, B., & Andersen, J. 2007, A&A, 537, 519

Howard, A., et al. 2011, arXiv:1103.2541

Howard, A., et al. 2010, Science, 330, 653

Huber, D., et al. 2010, ApJ, 723, 1607

Isaacson, H., & Fischer, D. 2010, ApJ, 725, 875

Jackson, B., Barnes, R., & Greenberg, R. 2009, ApJ, 698, 1357

Johnson, J. A., Butler, R. P., Marcy, G. W., Fischer, D. A., Vogt, S. S., Wright, J. T., & Kathryn, M. G. 2007, ApJ, 670, 833

Johnson, J., Aller, K., Howard, A., & Crepp, J. 2010, PASP, 122, 233

Kasting, J. F., Whitmire, D. P., & Reynolds, R. T. 1993, Icarus, 101, 108

Kennedy, G. M., & Kenyon, S. J. 2008, ApJ, 682, 1264

Koch, D., et al. 2010, ApJ, 713, L79

Lada, C. J. 2006, ApJ, 640, L63

Laughlin, G., Bodenheimer, P., & Adams, F. C. 2004, ApJ, 612, L73

Lee, Y., Beers, T., An, D., Ivezic, Z., & Just, A. 2011, ApJ, 738, 187

Lépine, S., & Gaidos, E. 2011, AJ, 142, 138

Lépine, S., & Shara, M. M. 2005, AJ, 129, 1483

Lissauer, J., et al. 2011, arXiv:1102.0543

Mamajek, E., & Hillenbrand, L. 2008, ApJ, 687, 1264

Marcy, G., & Butler, R. 1992, PASP, 104, 270

Mayor, M., et al. 2009, A&A, 507, 487

Moorhead, A., et al. 2011, ApJSS, 197, 1

Morton, T., & Johnson, J. 2011, ApJ, 738, 170

Muirhead, P., Hamren, K., Schlawin, E., Rojas-Ayala, B., Covey, K., & Lloyd, J. 2011, arXiv:1109.1819

Pierrehumbert, R., & Gaidos, E. 2011, ApJ, 734, L13

Raymond, S. N., Quinn, T., & Lunine, J. I. 2004, Icarus, 168, 1

Rogers, L. A., Bodenheimer, P., Lissauer, J. J., & Seager, S. 2011, ApJ, 738, 59

Schneider, J., Dedieu, C., Le Sidaner, P., Savalle, R., & Zolutukhin, I. 2011, A&A, 532, id.A79

Seager, S., Kuchner, M., Hier-Majumder, C. A., & Militzer, B. 2007, ApJ, 669, 1279

Valenti, J., & Piskunov, N. 1996, A&ASS, 118, 595

Vanhollebeke, E., Groenewegen, M. A. T., & Girardi, L. 2009, A&A, 498, 95

Verner, G. A., et al. 2011, ApJ, 738, L28

Vogt, S., et al. 1994, in Proc. SPIE Instrumentation in Astronomy VIII, ed. D. L. Crawford & E. R. Craine (SPIE), 362

Winn, J., et al. 2011, ApJ, 737, L18

Wolfgang, A., & Laughlin, G. 2011, arXiv:1108.5842

Zechmeister, M., Kürster, M., & Endl, M. 2009, A&A, 505, 859

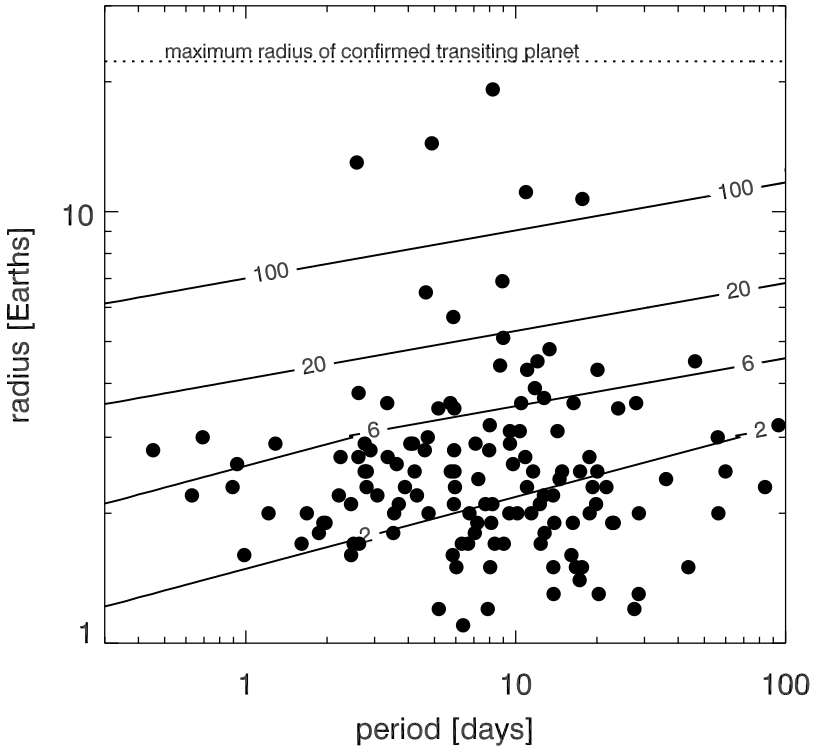

Fig. 1.— *Kepler* candidates plotted by orbital period and planet radius R_p, and contours of constant radial velocity variation (RMS = 2, 6, 20, 100 m s^{-1}) assuming a circular orbit, orbital inclination of 60°, and a mass given either by an average of confirmed transiting planets with similar radius (if R_p >3R$_\oplus$) or proportional to radius squared (if R_p <3R$_\oplus$). If the small planets are rocky then mass will be higher (proportional to R_p^4) and the RV RMS contours will be lower. Although many *Kepler* planets would be very difficult to individually detect (RMS < 6 m s^{-1}), they will aggregately contribute to significant RV variation, especially if they are composed primarily of rock and metal.

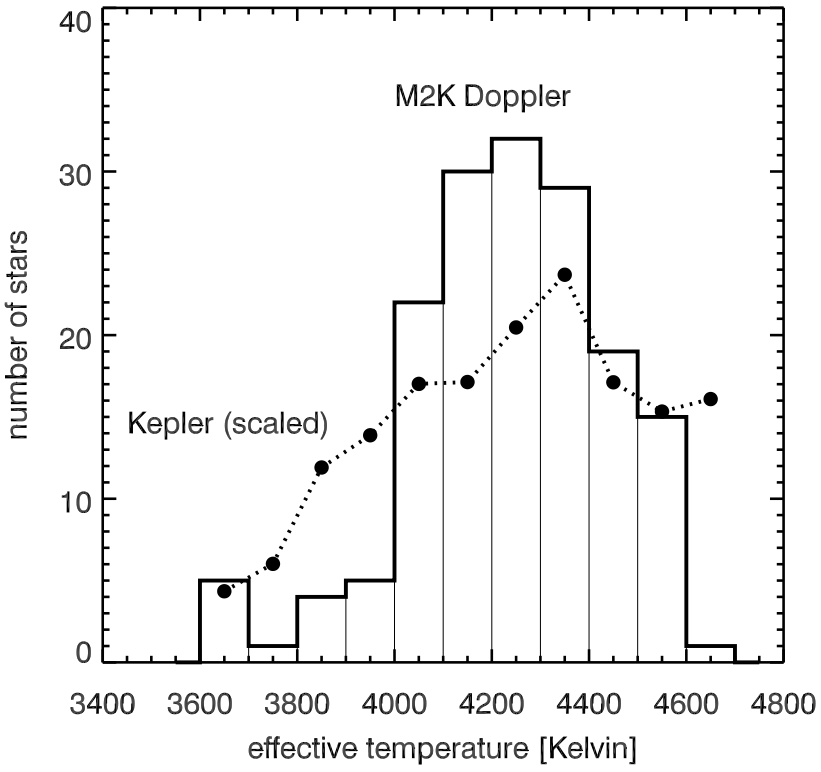

Fig. 2.— Distribution of effective temperatures in the M2K Doppler survey (bars) and *Kepler* Quarter 2 target catalog (dotted line) in the range 3660-4660 K. This range was chosen to maximize the similarity between the distributions as measured by the Kolmogorov-Smirnov test.

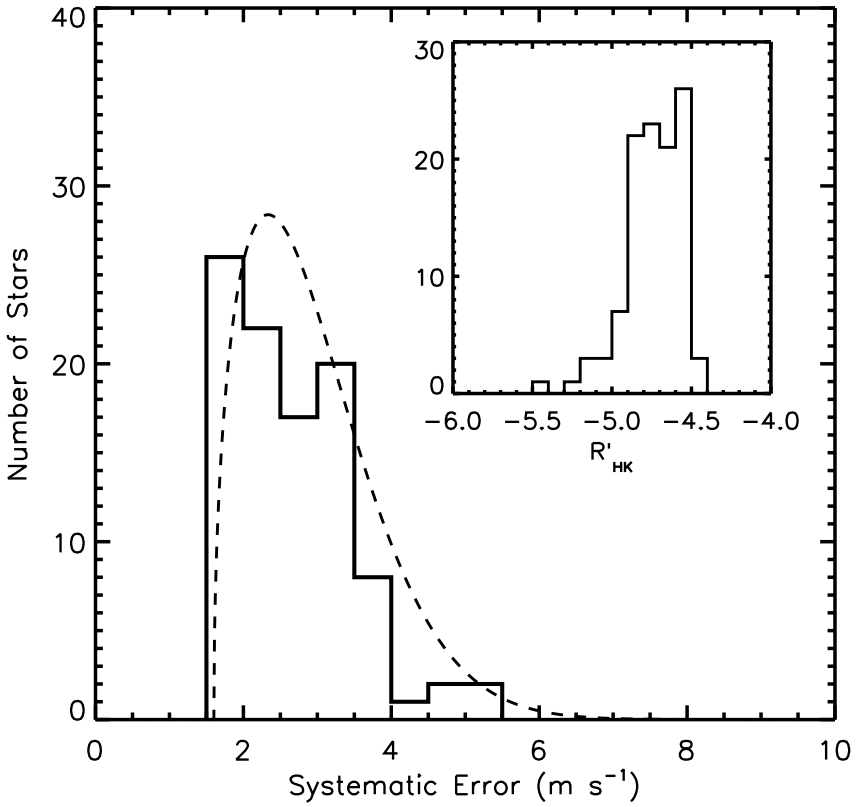

Fig. 3.— Predicted systematic error (instrument and stellar jitter) of Doppler measurements for 100 M2K stars based on $B - V$ color and emission in the H and K lines of Ca II. The dashed line is a best-fit noise model with a uniform instrument error of 1.6 m s^{-1} RMS added in quadrature to Rayleigh-distributed stellar jitter with $\sigma_0 = 1.7$ m s^{-1}. The distribution of Ca II HK emission, parameterized by the R'_{HK} index, is plotted in the inset. The median R'_{HK} of the sample is -4.70, corresponding to an age of about 3 Gyr (Mamajek & Hillenbrand 2008).

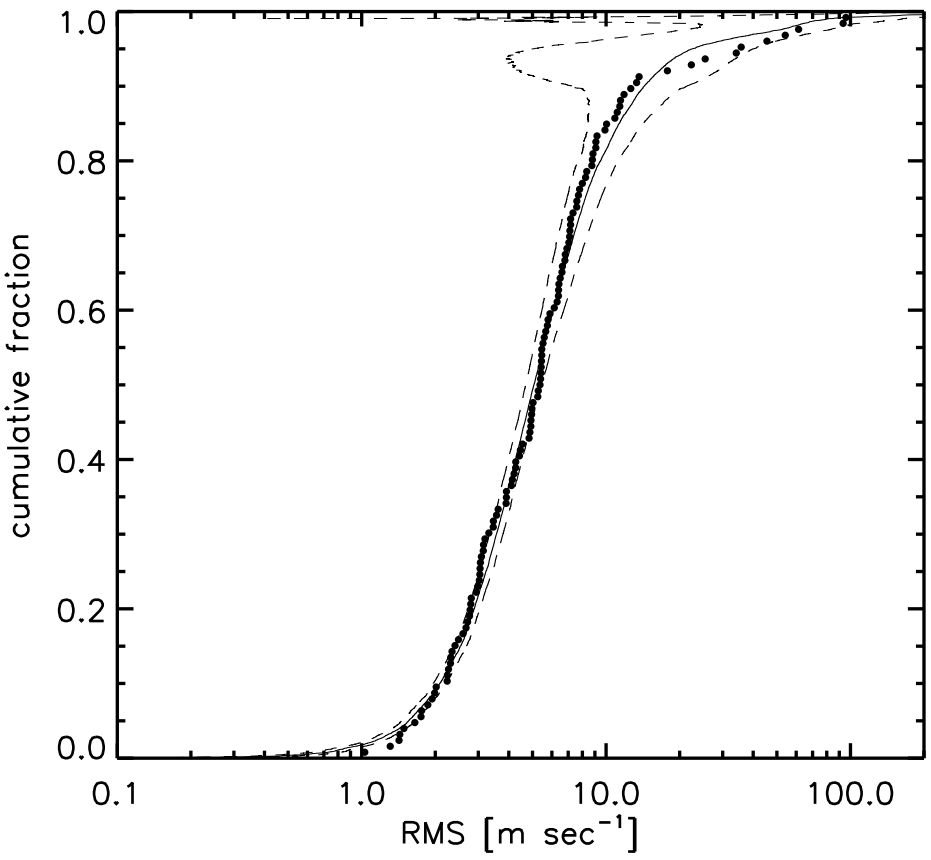

Fig. 4.— Cumulative distribution of RV RMS (points) in M2K stars with $T_e = 3660-4660$ K. The solid line is a model based on *Kepler* radii with Rayleigh-distributed systematic noise ($\sigma_0 = 2.6$ m s^{-1}), *Kepler* detection efficiency factor $C = 0.5$, binary cut-off $B = 110$ m s^{-1}, and power-law mass-radius relation with index $\alpha = 3.85$ for planets with $R_p \leq 3\mathrm{R}_\oplus$. The observations and model have a two-sided Kolmogorov-Smirnov probability of 93% that they could be drawn from the same population. The dashed lines are 95% confidence intervals for uncertainties generated by the finite size of the *Kepler* sample. These intervals are illustrative; cumulative distributions do not reverse.

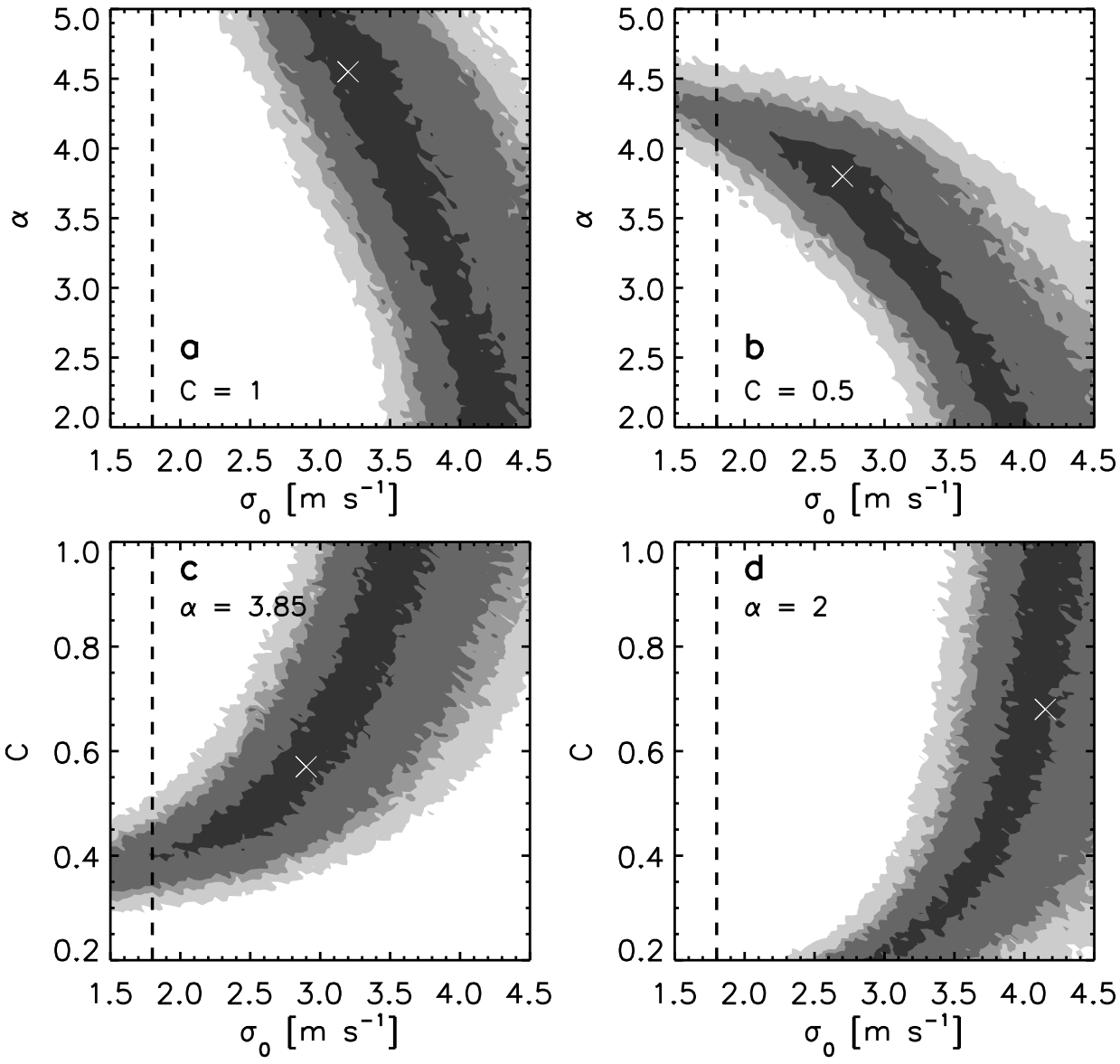

Fig. 5.— Kolmogorov-Smirnov probability for our *Kepler*/M2K comparison as it varies with jitter parameter σ_0, mass-radius relation power law index α, and *Kepler* detection efficiency C. Contours (lightest to darkest) are K-S probabilities of 0.01, 0.05, 0.1, and 0.5, representing confidence intervals of 99%, 95%, 90%, and 50%. The X marks the location of maximum probability, and the vertical dashed line marks $\sigma_0 = 1.8$ m s^{-1}, the value derived from observations and expected based on the distribution of Ca II HK emission among M2K stars. Panel (a) plots K-S probabilities with σ_0 and α assuming a *Kepler* detection effiency of $C = 1$; (b) same as (a) but with $C = 0.5$; (c) distribution with σ_0 and C for a rocky planet MRR ($\alpha = 3.85$); (d) same as (c) except for a notional gas-rich planet MRR ($\alpha = 2$).

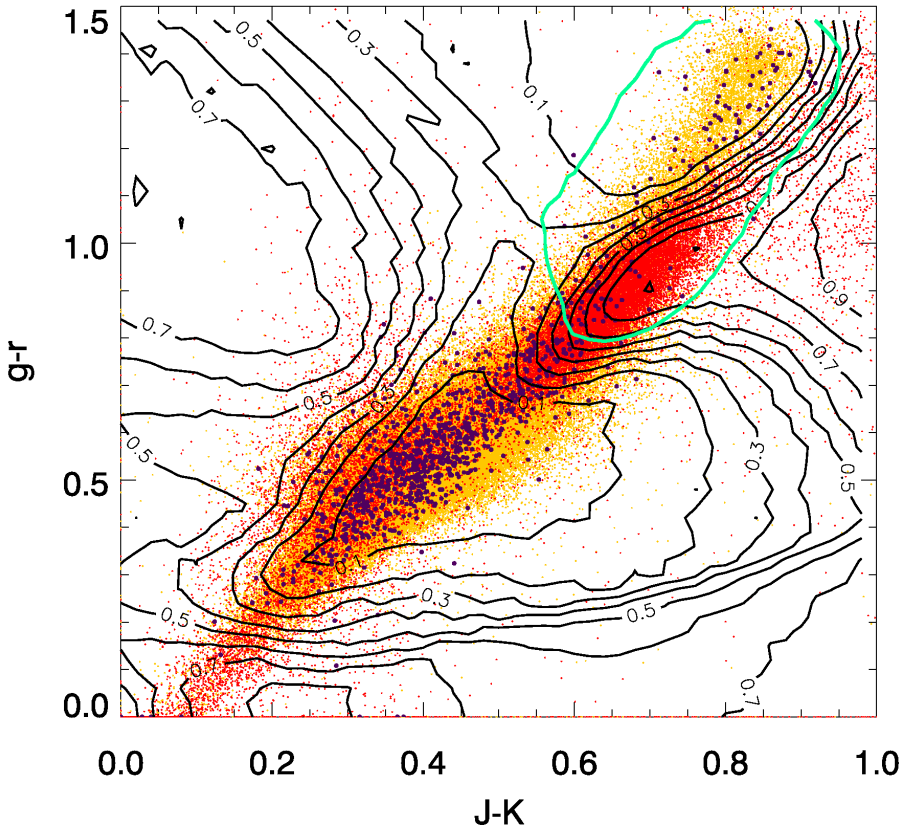

Fig. 6.— Color-color (SDSS $g-r$ and 2MASS $J-K$) diagram of *Kepler* target stars. Yellow and red points represent stars with estimated $\log g > 4$ (putative dwarfs) and $\log g < 4$ (putative giants or subgiants), respectively. Black contours are of constant (sub)giant fraction and the green contour encircles 90% of stars with $T_e = 3660 - 4660$ K. The large purple points are the host stars of planet candidates. The main sequence and giant branches intersect in the region of color-color space occupied by late K stars. This region appears to be deficient in planet candidates and those present are found where the (sub)giant fraction is least. This suggests that many putative dwarf stars in this region may be misclassified subgiants or giants, around which planets would be more difficult or impossible for *Kepler* to detect.

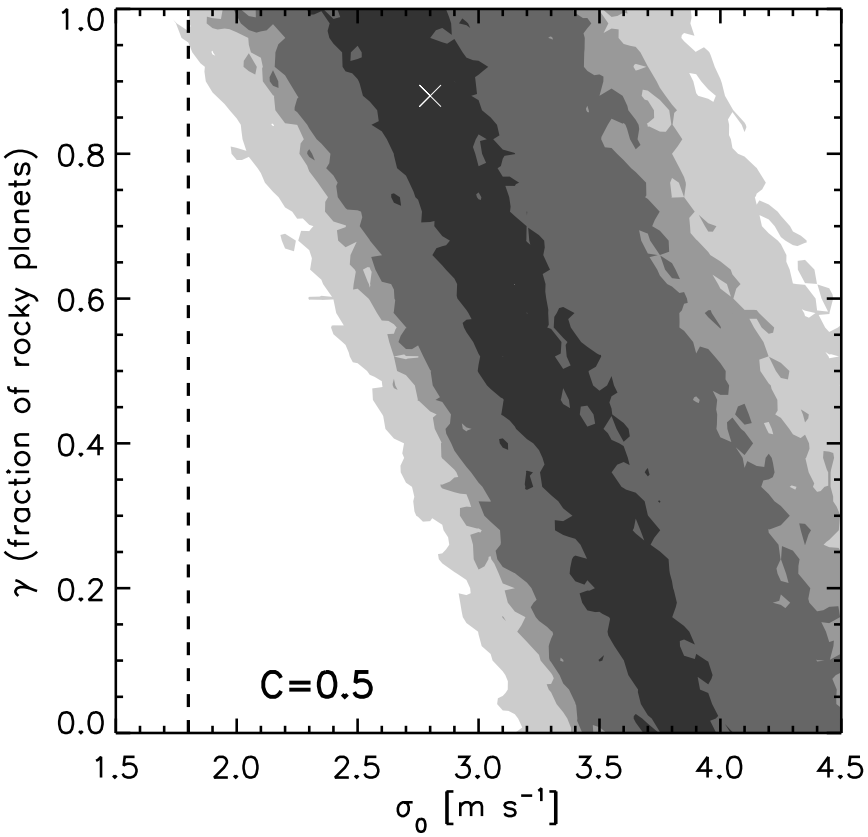

Fig. 7.— Kolmogorov-Smirnov probabilities vs. jitter magnitude σ_0 and fraction γ of rocky ($\alpha = 3.85$) planets vs. gas-rich ($\alpha = 2$) planets, assuming a *Kepler* completeness $C = 0.5$. Countours (lightest to darkest) are K-S probabilities of 0.01, 0.05, 0.1, and 0.5, representing confidence intervals of 99%, 95%, 90%, and 50%. The X marks the location of maximum probability. The vertical dashed line at 1.8 m s^{-1} marks the expected value of σ_0 for M2K stars.

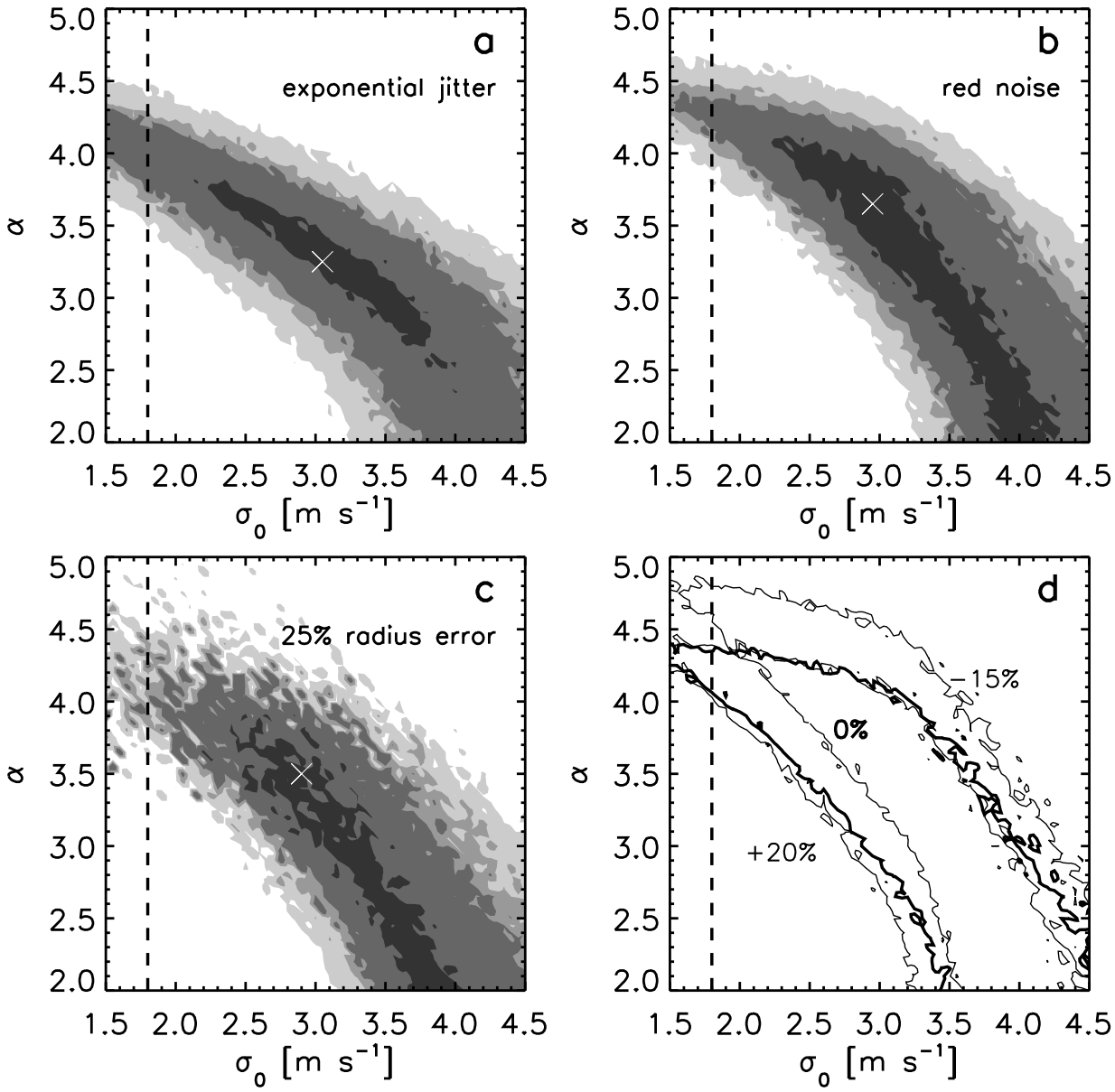

Fig. 8.— Sensitivity of our results to different assumptions in the model used to translate *Kepler* radii into Doppler radial velocity variance. All calculations assume $C = 0.5$ and these plots should be compared to Figure 5b. In (a) we use an exponential rather than a Rayleigh function to describe the distribution of jitter RMS among stars. In (b) instrument noise is modeled as being correlated on a timescale of 20 d. In (c) 25% gaussian error is added to *Kepler* stellar radius estimates. In (d) the radii of *Keper* stars (and planets) are uniformly increased by 20% or decreased by 15% from KIC values (heavy line). See text for justification of these choices. For clarity, only the 90% confidence contours are shown in the last panel.

Table 1. Radial velocity statistics of 150 stars with T_e=3660-4660 K in the M2K Survey

Star	Measurements	Stand. Dev. m s^{-1}	Formal Error m s^{-1}
1	18	3.19	1.30
2	8	5.42	1.58
3	9	2.94	1.07

Note. — Table 1 is published in its entirety in the electronic edition of the *Astrophysical Journal*.